



A01-34112

AIAA 2001-3326

Electron Energy Distribution Function
in a Hall Discharge Plasma

N. B. Meezan and M. A. Cappelli
Mechanical Engineering Department
Stanford University
Stanford, CA

**37th AIAA/ASME/SAE/ASEE
Joint Propulsion Conference and Exhibit
8-11 July 2001
Salt Lake City, Utah**

Electron Energy Distribution Function in a Hall Discharge Plasma

Nathan B. Meezan[†] and Mark A. Cappelli[‡]

Mechanical Engineering Department, Stanford University, Stanford, California 94305-3032

The role of inelastic collisions in Hall thruster operation is studied through simulation of the electron energy distribution function (EEDF) inside the thruster channel. The electron Boltzmann equation is solved using the Lorentz approximation (two-term expansion) and the “local-field” approximation. The resultant zero-dimensional Boltzmann equation takes into account inelastic losses due to ionizing collisions and wall-collisions. Secondary electrons from ionization and wall-collisions are also included in the model. Electron continuity is used to calculate the sheath potential at the insulator walls. Results show an EEDF cut off at high energy due to electron loss to the walls. Secondary and scattered electrons from ionization provide a large population of low-energy electrons. The calculated EEDFs agree well with experimental electron temperature data when an experimentally-determined effective collision frequency is used for electron momentum transport. Predicted values for the wall-sheath potential agree with results from a charge-balance model, except where said model predicts sheath collapse.

I. INTRODUCTION

Hall discharges (Hall thrusters) are presently under development for use in space propulsion applications. The Hall thruster is essentially a shaped-field accelerator, using applied potentials and magnetic fields to produce a high specific impulse, low-density plasma flow. The shape of the electric field, the Ohmic losses, and the locations of the ionization zone and acceleration zone inside the thruster are coupled to the applied fields through the plasma conductivity. The electrons in Hall discharges exhibit characteristic cross-field transport, which is believed to be enhanced by fluctuations in the electric field and plasma density [1]. Collisions with the thruster channel walls also play an important role in discharge operation.

Several researchers have had success modeling the plasma inside the Hall discharge (and similar discharges) with hybrid fluid-particle codes [2-5] and full particle codes [6]. With the hybrid fluid-particle in cell (PIC) codes, some investigators have used an anomalous Bohm conductivity in order to accurately reproduce discharge operation [5], while others have relied on a model for electron-wall scattering [3,4]. Many of these efforts have had difficulty reproducing the location of the ionization zone inside the thruster channel. We believe that this may be due to a non-Maxwellian electron energy distribution function (EEDF) in the discharge plasma. Electrostatic probe measurements of the EEDF have shown significant departures from Maxwellian behavior [7-10.]. We [11] and others [10] have also observed behavior that may be attributable to a non-Maxwellian EEDF in optical emission experiments.

Inelastic processes such as ionization and electron-wall-loss collisions are very important in the low-pressure Hall thruster plasma. In this study, we attempt to use numerical solutions of the electron Boltzmann equation to help understand the role of electron-wall collisions in forming the EEDF. We also hope to gain insight into the importance of electron-wall interactions to the cross-field plasma conductivity. The strong coupling between the EEDF and inelastic processes allows us to study the impact of these processes on thruster performance without complex models. As a result of an extensive diagnostic effort put forth to measure the plasma properties inside a laboratory Hall thruster [12,13], we have a large amount of data to aid us in this effort. As a first effort, we simply use measured plasma properties as inputs to directly solve the Boltzmann equation. Later studies for operating conditions without experimental data will require coupling the electron Boltzmann equation and its moments to a fluid, hybrid, or PIC simulation.

II. THEORY

The steady-state Boltzmann equation for the electrons can be written as

$$\mathbf{c} \cdot \nabla_x f - \frac{e}{m} (\mathbf{E} + \mathbf{c} \times \mathbf{B}) \cdot \nabla_c f = \left(\frac{\delta f}{\delta t} \right)_{coll}, \quad (1)$$

where f is the electron velocity distribution function (EVDF), \mathbf{c} is the vector electron velocity, ∇_x is the gradient operator with respect to positional space, and ∇_c is the gradient in velocity space. We proceed to a solution of this equation following several approximations. The EVDF f is separated into a component that is predominantly isotropic, f_0 , and components that skew the distribution in the direction of the electric field and the $\mathbf{E} \times \mathbf{B}$ drift [14, 15]:

$$f(\mathbf{c}) = f_0(c) + (\mathbf{c} \cdot \mathbf{E}) f_1(c) + [\mathbf{c} \cdot (\mathbf{B} \times \mathbf{E})] f_2(c). \quad (2)$$

[†] Research Assistant, Student Member AIAA

[‡] Associate Professor, Member AIAA

Copyright © 2001 by Stanford University. Published by the American Institute of Aeronautics and Astronautics, Inc. with permission.

The functions f_1 and f_2 are also isotropic, and when weighted by cE and $c(\mathbf{B} \times \mathbf{E})$, result in a small perturbation on the predominantly isotropic core. This model is therefore not appropriate for EVDFs with extreme anisotropy due to high drift energies or “beam-like” electrons streaming from the cathode neutralizer, e.g. ref. [7].

The directions of the electric field \mathbf{E} and magnetic field \mathbf{B} are taken as purely axial (\mathbf{z}) and radial (\mathbf{r}), respectively. We then neglect spatial gradients in the axial direction by making the “local field” approximation. The cyclotron radius of the electrons in the Hall discharge is 10-1000 times smaller than the electron mean-free-path, except very near the anode. Thus, the EEDF is formed locally, at distances below the mean-free-path. In other words, due to magnetic confinement, an electron reaches equilibrium with the local fields on time scales shorter than that which controls diffusion across a characteristic length scale of the plasma. The axial variation of the EEDF is determined solely by the axial change in plasma properties. This approach has been successfully applied to the determination of the EEDF in a cylindrical magnetron [16], a discharge similar to the Hall thruster in size, pressure, and magnetic field-strength. We also treat the plasma as uniform in the azimuthal direction due to symmetry, and in the radial direction, as electrons can freely diffuse along radial magnetic field lines. For a more detailed explanation of the local and non-local approaches to solving the Boltzmann equation, see ref. [17].

After removing the spatial gradient term, the solution proceeds by substituting the perturbation expression Eq. (2) into Eq. (1), expanding the right-hand-side as a series of collision integrals, and simplifying the equation to a scalar expression for the isotropic EVDF f_0 . This laborious procedure is detailed for elastic collisions only in ref. [15] and for elastic and inelastic collisions in ref. [14] and will not be repeated here. In our results, the temperature of the background xenon neutrals is also neglected. After adding the wall-loss collisions and separating the elastic and inelastic terms, the equation becomes

$$\begin{aligned} & \frac{1}{3} \left(\frac{eE}{mc} \right)^2 \frac{d}{dc} \left[c^2 \left(\frac{N\sigma_m c}{\omega^2 + (N\sigma_m c)^2} \right) \frac{df_0}{dc} \right] + N \frac{m}{Mc^2} \frac{d}{dc} \left[c^4 \sigma_m f_0 \right] \\ & = -Nc \left[\sigma_{ij} \left(c_{ij}' \right) \left(\frac{c_{ij}'}{c} \right)^2 f_0 \left(c_{ij}' \right) - \sigma_{ij}(c) f_0(c) \right] + v_{wall} f_0, \end{aligned} \quad (3)$$

where N is the neutral gas density, m and M are the electron and xenon atom masses respectively, ω is the electron cyclotron frequency, σ_m is the momentum-transfer cross-section for electron-neutral collisions, and σ_{ij} is the cross-section for an inelastic process from energy level i to energy level j . The velocity after a de-exciting collision is defined as

$$c_{ij}' = \sqrt{c^2 + \frac{2\varepsilon_j}{m}}, \quad (4)$$

where ε_j is the excitation threshold energy. For this study, we restrict the inelastic collisions to ionization and wall-loss collisions and their corresponding secondary electron processes. Other inelastic electron-neutral collisions, as well as electron-electron and electron-ion collisions, have been neglected. These processes may be added to the model in a later study.

Moving into energy-space, we substitute the kinetic energy $u = kc^2$, where the constant k is defined such that u is expressed in eV. The subscript is dropped from the isotropic EVDF f_0 , and we let $f(c) = f(u)$ for convenience. This simplifies to

$$\begin{aligned} & \frac{4}{3} \left(\frac{eE}{m} \right)^2 k^2 \frac{d}{du} \left[\left(\frac{N\sigma_m u^2}{k\omega^2 + N^2\sigma_m^2 u} \right) \frac{df}{du} \right] + N \frac{2m}{M} \frac{d}{du} \left[u^2 \sigma_m f \right] \\ & = uN\sigma_i(u)f(u) - N(u+u_i)\sigma_i(u+u_i)f(u+u_i) + \sqrt{k}v_{wall}(u)f(u). \end{aligned} \quad (5)$$

From left to right, the terms in the equation represent Joule heating, elastic collisions, loss of electrons due to ionization, return of electrons from ionizing collisions, and loss of electrons to the wall. Equations (3) and (5) assume that electrons are transported across the magnetic field lines primarily by elastic collisions with xenon atoms. Alternatively, an *ad hoc* experimentally-determined “effective” collision frequency can be used by substituting v_{eff} for $N\sigma_m c$ in Eq. (3). The effective collision frequency attempts to include effects left out by this model, such as electron-wave interactions. These two momentum-transport models will be compared later in the paper.

The wall-loss collision frequency v_{wall} must take into account both the transit-time of electrons in the discharge channel and the sheath formed at the channel wall. We write the characteristic rate at which an electron of velocity c reaches the wall as c/w , where w is the (radial) width of the discharge channel. Since the magnetic field lines are almost radial and the mean-free-path is on the order of the channel width, electrons are free to stream to the wall; however, only electrons with energies greater than the wall-sheath potential will actually reach the wall. Electrons of lower energy should scatter off the sheath nearly elastically. So, the final expression for the rate of wall-loss collisions is

$$v_{wall} = H(u - e\phi_{wall}) \frac{c}{w} = H(u - e\phi_{wall}) \frac{1}{w} \sqrt{\frac{u}{k}}, \quad (6)$$

where H is the Heaviside step-function and ϕ_{wall} is the magnitude of the (negative) sheath potential.

At this point, we introduce the secondary electron terms, following ref. [18]. We define q as the cross-section for producing secondary or scattered electrons of particular energies. The collision term for ionization is then expressed:

$$\begin{aligned} \left(\frac{\delta f(u)}{\delta t} \right)_{coll.} &= \frac{cN}{u} \int_{2u+u_i}^{\infty} u' q_{sec}^i(u', u) f(u') du' \\ &+ \frac{cN}{u} \int_{u+u_i}^{2u+u_i} u' q_{sca}^i(u', u) f(u') du' - cN \sigma_I(u) f(u). \end{aligned} \quad (7)$$

The first two terms on the right-hand-side are the source terms for secondary and scattered electrons, respectively. The third term is the ionization loss term. The variable u' is a dummy variable of integration. The integrals involving q can be simplified using delta-function expressions:

$$\begin{aligned} q_{sec}^i(u', u) &= \sigma_I(u') \delta(u - \tilde{u}), \quad \text{and} \\ q_{sca}^i(u', u) &= \sigma_I(u') \delta[u - (u' - u_i - \tilde{u})]. \end{aligned} \quad (8)$$

Here, δ is the Dirac delta function and \tilde{u} is the energy of the secondary electron. The value

$$\tilde{u} = \left(\frac{u' - u_i}{2} \right), \quad (9)$$

representing a case in which the energy remaining from the inelastic collision is divided equally between the secondary and scattered electrons, will be used here.

We can apply the same formalism to wall collisions by removing the scattered electron term and assuming that electrons emitted from the wall have negligible energy, i.e., setting $\tilde{u} = 0$. The rate of secondary production from the wall is given by

$$v_{sec} = v_{wall}(u) \gamma(u - e\phi_{wall}), \quad (10)$$

where we use γ as the secondary electron emission coefficient to avoid confusion with the Dirac delta function. In this simple model, γ is evaluated at the kinetic energy less the sheath-potential energy, as the electron loses this energy before striking the wall.

Combining Eqs. (6-10) and incorporating them into the Boltzmann equation, we arrive at:

$$\begin{aligned} \frac{4}{3} \left(\frac{eE}{m} \right)^2 k^2 \frac{d}{du} \left[\left(\frac{N\sigma_m u^2}{k\omega^2 + N^2\sigma_m^2 u} \right) \frac{df}{du} \right] &+ N \frac{2m}{M} \frac{d}{du} [u^2 \sigma_m f] \\ &= Nu \sigma_I(u) f(u) - 2N(2u + u_i) \sigma_I(2u + u_i) f(2u + u_i) + \\ &\frac{u}{w} H(u - e\phi_{wall}) f(u) - \delta(u) \int_{e\phi_{wall}}^{\infty} \frac{u'}{w} \gamma(u' - e\phi_{wall}) f(u') du'. \end{aligned} \quad (11a)$$

The ionization return term represents two electrons at equal energies. The wall-secondary term is equivalent to returning all secondary electrons from the wall to the EVDF at zero energy. The equation must satisfy one boundary condition at infinity,

$$f \rightarrow 0 \quad \text{as} \quad u \rightarrow \infty, \quad (11b)$$

and the normalization condition,

$$\int_0^{\infty} \sqrt{u} f du = \int_0^{\infty} F du = 1. \quad (11c)$$

The equation is now ready to be solved numerically.

III. NUMERICAL SOLUTION

It is convenient to re-write Eq. (11a) using collision operators before proceeding with the numerical solution [16]:

$$D(u) = \frac{4}{3} \left(\frac{eE}{m} \right)^2 k^2 \left(\frac{N\sigma_m u^2}{k\omega^2 + N^2\sigma_m^2 u} \right) \quad (12a)$$

for electron transport by elastic collisions only, or

$$D(u) = \frac{4}{3} \left(\frac{eE}{m} \right)^2 k^2 u^{\frac{3}{2}} \left(\frac{v_{eff}}{v_{eff}^2 + \omega^2} \right) \quad (12b)$$

for an experimental (energy-independent) collision-frequency. Similarly,

$$G(u) = N \frac{2m}{M} u^2 \sigma_m, \quad \text{or} \quad (13a)$$

$$G(u) = \frac{2m}{M} k^{\frac{1}{2}} u^{\frac{3}{2}} v_{eff}. \quad (13b)$$

$$J(u) = Nu \sigma_I(u), \quad (14)$$

$$W(u) = \frac{u}{w} H(u - e\phi_{wall}), \quad (15)$$

$$I(u) = N(u + u_i) \sigma_I(u + u_i) f(u + u_i) \quad (16a)$$

when neglecting secondary electrons from ionization, or

$$I(u) = 2N(2u + u_i) \sigma_I(2u + u_i) f(2u + u_i) \quad (16b)$$

when including ionization secondaries, and

$$S(u) = \delta(u) \int_{e\phi_{wall}}^{\infty} \frac{u'}{w} \gamma(u' - e\phi_{wall}) f(u') du'. \quad (17)$$

In this notation, Eq. (11) becomes

$$\begin{aligned} \frac{d}{du} \left[D(u) \frac{df}{du} \right] &+ \frac{d}{du} [G(u) f] \\ &- J(u) f(u) - W(u) f(u) = -I(u) - S(u). \end{aligned} \quad (18)$$

This equation is discretized on an equidistant grid of K points using 2nd-order accurate central differences and written as a matrix equation $\mathbf{A} \mathbf{f} = \mathbf{b}$. The boundary condition at infinite energy is expressed as $f_K = 0$. The maximum energy u_K must be large enough that the error in the boundary condition does not effect the solution at low energy. The normalization condition is expressed using Simpson's rule along the top row of \mathbf{A} and \mathbf{b} . The resultant

matrix \mathbf{A} is tri-diagonal except for the first row and is easily inverted:

$$\begin{aligned} & \left(\frac{1}{h^2} D_i - \frac{1}{4h^2} (D_{i+1} - D_{i-1}) - \frac{1}{2h} G_i \right) f_{i-1} \\ & + \left(-\frac{2}{h^2} D_i - \frac{1}{2h} (G_{i+1} - G_{i-1}) - J_i - W_i \right) f_i \\ & + \left(\frac{1}{h^2} D_i + \frac{1}{4h^2} (D_{i+1} - D_{i-1}) - \frac{1}{2h} G_i \right) f_{i+1} = -I_i - S_i. \end{aligned} \quad (19)$$

The ionization return term I is evaluated off the grid, so it appears on the right-hand-side of the matrix equation with the wall-secondary term S , which requires an integral of the EVDF. The wall-collision terms W and S also depend on the potential at the wall sheath. Therefore, the solution is an iterative procedure [19].

The code takes as inputs plasma properties derived from optical and probe experiments performed on a laboratory Hall thruster with an alumina (Al_2O_3) channel. In total, solution of Eq. (11) requires, as a function of the axial coordinate z , the electric field E , magnetic field B , neutral xenon density N , and effective collision frequency ν_{eff} . The electron density n_e and electron current I_e are also needed to find the wall-sheath potential. These data are summarized in ref. [20]. Details of the experiments can be found in refs. [12, 13]. For these experiments, the thruster was operated with a peak magnetic field-strength of 100 G and a mass flow rate of 2 mg/s xenon. Cross-section data were taken from the SIGLO database [21]. We approximated the secondary electron-emission coefficient for alumina as a line passing through $\gamma=0$ at zero energy and $\gamma=1$ at the first crossover, 25 eV [22].

The wall-sheath potential is calculated from electron continuity, so a detailed sheath model is unnecessary. Electron production by ionization is balanced by the net outflow of electron current and the net loss of electrons to the wall:

$$\begin{aligned} & \frac{n_e A_{\text{chan}}}{\sqrt{k}} \int_0^\infty N u \sigma_i(u) f(u) du - \frac{1}{e} \frac{dI_e}{dz} \\ & = \frac{n_e A_{\text{chan}}}{\sqrt{k}} \int_{e\phi_{\text{wall}}}^\infty \frac{u}{W} (1 - \gamma(u - e\phi_{\text{wall}})) f(u) du, \end{aligned} \quad (20)$$

where A_{chan} is the cross-sectional area of the discharge channel. The wall-sheath potential is chosen on the grid.

The iteration, shown schematically in Fig. 1, proceeds as follows: First, the Eq. (19) is solved with no inhomogeneous terms. From the first solution f^1 , the wall potential is calculated from Eq. (20). The terms I and S are also calculated from the previous solution, using cubic-spline interpolation to evaluate off-grid points. Equation (19) is then solved including the inhomogeneous terms. This procedure is repeated until the relative error between two

successive solutions is below 10^{-5} , usually in 10-30 iterations.

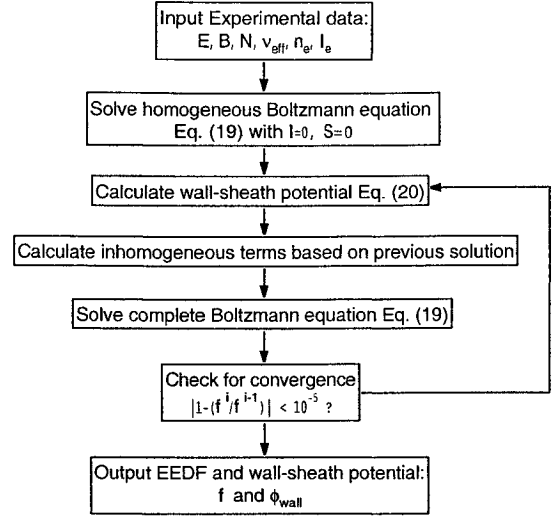


Fig. 1. Flow chart of numerical solution

IV. RESULTS

A. General results

Figure 2 shows the isotropic part of the EVDF f calculated using the effective collision frequency for momentum transfer for 200 V operation 15 mm upstream of the thruster exit. For ionization collisions only, the EVDFs are nearly Maxwellian, except near zero energy. Including secondary electrons from ionization results in more low-energy electrons in the distribution, decreasing the average energy. When wall-collisions are added to the model, the average energy decreases dramatically. At energies beyond the wall-sheath potential (~ 30 V for this case), the distribution falls off quickly as electrons are lost to the wall.

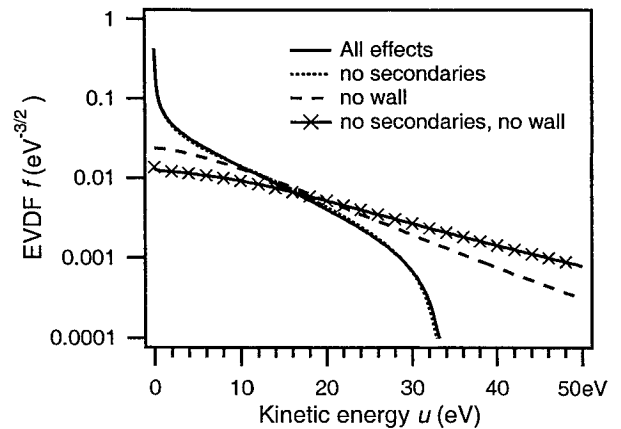


Fig. 2. Calculated EVDFs f for different inelastic collision models.

Surprisingly, re-injecting secondary electrons from the wall has no visible effect on the distribution. This fact is more apparent in Fig. 3, where the EEDF $F = \sqrt{u} f$ is plotted for

the same conditions. While including wall-secondaries has no effect, including secondary electrons from ionization does noticeably change the distribution. This result is primarily due to the fact that ionization produces more secondary electrons in the plasma than does wall-loss. As shown in Fig. 4, the ionization rate is greater than the wall-loss rate throughout most of the channel.

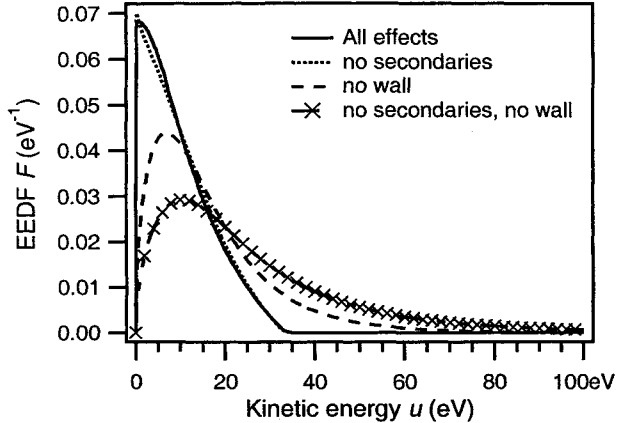


Fig. 3. Calculated EEDFs F for different inelastic collision models.

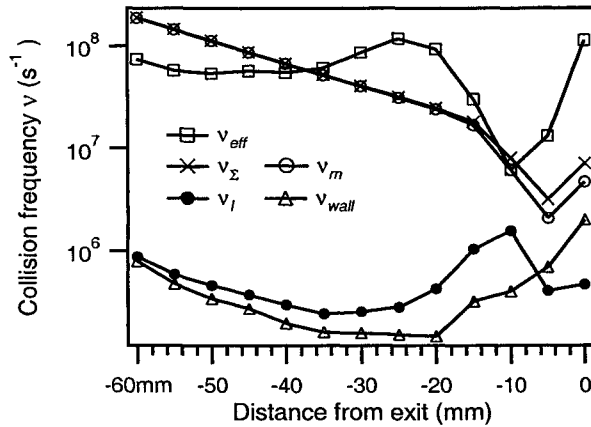


Fig. 4. Comparison of various collision frequencies inside the thruster channel at 200 V operation.

B. Comparison of momentum-transfer models

Figure 4 also compares the other collision-frequencies used or generated by the code. Here, ν_l and ν_m are the frequencies for ionization and elastic momentum-transfer collisions, respectively, as calculated using the SIGLO cross-sections; ν_{wall} is the bulk rate of wall-loss collisions, given by integrating Eq. (6) over F ; $\nu_z = \nu_m + \nu_l + \nu_{wall}$ is the total collision frequency; and ν_{eff} is the experimentally determined effective collision frequency. Elastic collisions with xenon neutrals dominate inelastic processes throughout the channel; thus, it is unlikely that wall-loss collisions and secondary electrons contribute greatly to electron momentum transfer in the discharge, at least at the operating conditions investigated here.

Near the anode, elastic collisions are clearly sufficient for electron momentum transfer in the discharge; however, within 30 mm of the thruster exit, elastic collisions cannot account for the measured cross-field electron transport. It is worth noting that the trend in ν_m with z is due almost entirely to the neutral gas density N , which was measured with great experimental uncertainty. The dip in ν_{eff} at $z = -10$ is less severe at other discharge operating conditions and is, as of yet, unexplained.

The differences between the two momentum models used for this study is also evident in Fig. 5. The EVDF calculated using ν_{eff} (for 200 V operation 15 mm upstream of the exit) agrees very well with a Maxwellian distribution at the experimental electron temperature, T_{exp} , even though the plasma properties used as inputs to the model depend very weakly on T_{exp} . Using only elastic collisions for momentum transport, the model cannot suitably reproduce the experimentally-observed electron temperature. At this time, using the experimentally-determined effective collision frequency ν_{eff} in the Boltzmann equation is appropriate. Including charged particle collisions in the model may resolve the discrepancy between ν_{eff} and ν_z . This will be investigated in a future study.

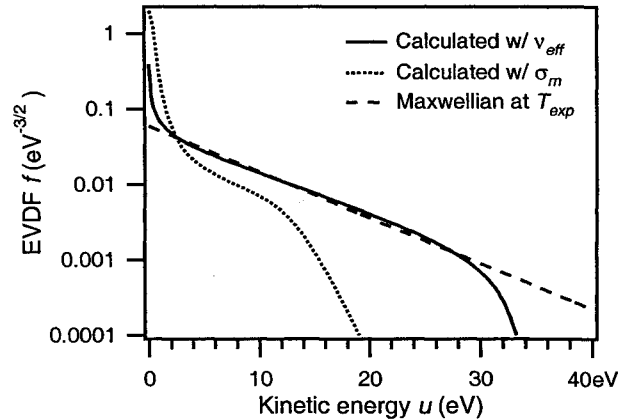


Fig. 5. Calculated EVDFs for different momentum-transfer models and comparison to Maxwellian distribution.

C. Deviation from Maxwellian

Considering the difficulty of obtaining the correct electron temperature from an experimental investigation (or from a full simulation) of a Hall discharge, it is important to ascertain the error implicit in the Maxwellian assumption. A closer look at Fig. 5 shows that the calculated EVDF agrees very well with a Maxwellian at T_{exp} at intermediate energies (15-45 eV), but deviates at extreme energies. Thus, the calculated distribution has a slightly lower mean energy than experiments suggest. This is better seen in Fig. 6, a comparison between the experimental and calculated electron temperatures, where the effective temperature is defined as that of a Maxwellian distribution with the same mean energy,

$$\bar{u}_{Max} = \frac{3}{2}k_B T_e \rightarrow k_B T_{eff} = \frac{2}{3}\bar{u} = \frac{2}{3} \int_0^{\infty} u F du \quad (21)$$

Near the exit plane, the temperatures agree fairly well. The large discrepancies near the anode are probably due to error in the neutral gas density N , as mention above.

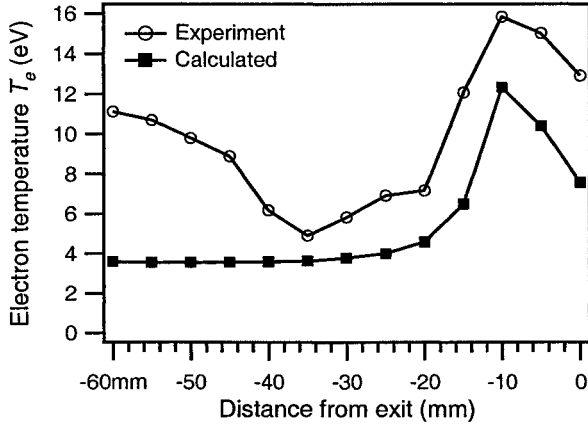


Fig. 6. Comparison of calculated to measured electron temperature

With this effective temperature, we can look at the impact of the shape of the calculated distribution on the ionization rate, v_i . Calculating v_i based on a Maxwellian at T_{eff} leads to an ionization rate 2-3 times lower than that predicted by the simulation, as shown in Fig. 7. Since the two distributions have the same mean energy, this difference is due entirely to the shape of the distribution: The low energy electrons in f bring down T_{eff} but do not play a role in ionization. The two rates do show very similar trends. Perhaps a medium between a full Boltzmann solver and the Maxwellian assumption would be suitable for most purposes.

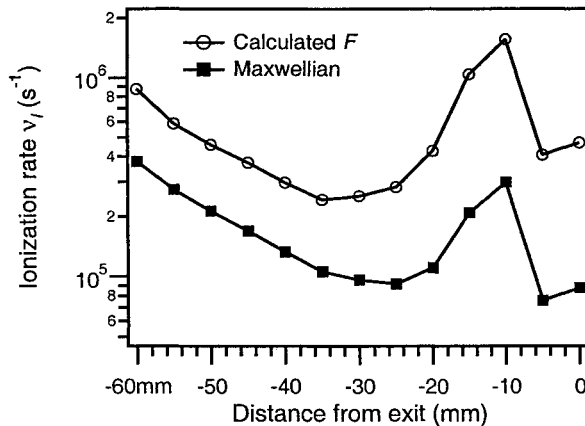


Fig. 7. Comparison of calculated ionization rate to that of a Maxwellian of equal mean energy.

D. Wall collision models

The simulation can also be used to compare the calculated wall-sheath potential and wall-loss rates to other

sheath models. One such model, proposed by Fife [3], uses an effective secondary-emission-coefficient defined by,

$$\Gamma_{sec} = \gamma_{eff} \Gamma_e = \gamma_{eff} \frac{\bar{c}_e}{4}, \quad (22)$$

where \bar{c}_e is the mean thermal speed of the electron. The coefficient γ_{eff} is found by computing the one-way-flux of a Maxwellian distribution multiplied by the function $\gamma(u)$. For γ linear with u , this leads to

$$\gamma_{eff} = \frac{2k_B T_e}{u_{cross}}, \quad (23)$$

where u_{cross} is the first cross-over energy of the material. The sheath potential is then found by balancing the net electron flux with the ion flux, assuming ions enter the sheath at the Bohm velocity:

$$\Gamma_{e,net} = (1 - \gamma_{eff}) \frac{\bar{c}_e}{4} n_e \exp\left(\frac{e\phi_{wall}}{kT_e}\right) = \Gamma_i = n_e \sqrt{\frac{k_B T_e}{M}} \quad (24a)$$

$$\rightarrow \phi_{wall} = -\frac{k_B T_e}{e} \ln \left[(1 - \gamma_{eff}) \sqrt{\frac{M}{2\pi m}} \right]. \quad (24b)$$

We neglect a factor of 0.61 due to the pre-sheath. The wall-sheath potential can then be calculated using the effective electron temperature defined above. This result are compared to the wall-sheath potential returned by the simulation in Fig. 8. The sheath model shows excellent agreement with the simulation except for two points near the discharge exit. When the argument of the logarithm in Eq. (24b) becomes zero, the sheath is neutralized by secondary electrons and collapses. This effect brings down the sheath potential at high temperature, severely increasing the predicted rate of electron loss to the wall.

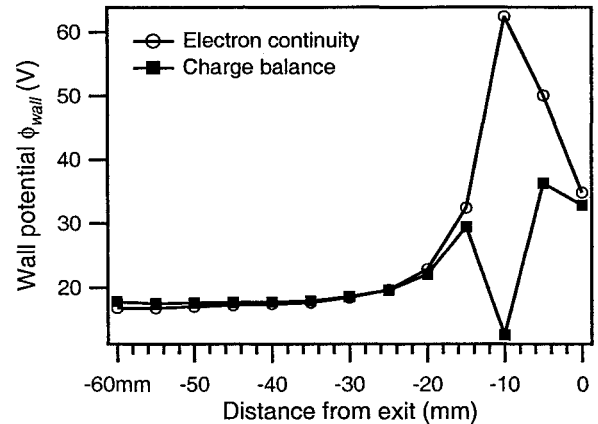


Fig. 8. Comparison of wall potential models.

From Eq. (24a), this rate is given by,

$$v_{wall} = \frac{\bar{c}_e}{4} \exp\left(\frac{e\phi_{wall}}{kT_{eff}}\right). \quad (25)$$

Figure 9 shows that this wall-loss rate is consistently higher than that returned by the EEDF simulation. Where

the sheath begins to collapse, the wall-loss rate can exceed the elastic collision frequency and contribute to cross-field transport. This situation is avoided in the EEDF simulation because the secondary emission coefficient is evaluated at the kinetic energy less the wall potential energy. The sheath potential increases with the average electron energy, but the secondary emission rate does not correspondingly rise. The secondary emission coefficient is measured in ref. [22] on an uncharged sample, so the slowing of electrons by the sheath must be taken into account separately.

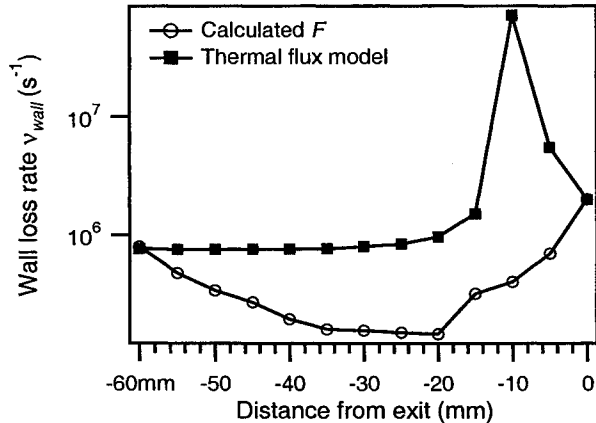


Fig. 9. Comparison of wall-loss models.

V. SUMMARY

The solutions to the Boltzmann equation presented here suggest that wall collisions are not important to cross-field electron-transport. They do, however, play a critical role in the discharge electron energy balance. By selectively removing high energy electrons from the distribution, wall-collisions significantly lower the mean electron energy and, combined with ionization, skew the distribution towards low energies. At intermediate energies between the wall-sheath potential and the ionization threshold, the EEDF behaves essentially like a Maxwellian distribution. This suggests that assuming a Maxwellian distribution for the electrons is acceptable, as long as your experiment samples electrons in this range. In fact, this is probably more accurate than using a Maxwellian at the true average energy for calculating the ionization rate. For experiments (or models) that depend on electrons of very low or very high energy, the Maxwellian assumption will not be suitable. Results of the simulation dealing with electron-wall interaction agree quite well with a simple model based on charge neutrality at the wall, as long as the wall-sheath does not (or is not allowed to) collapse. Accurate values for and correct evaluation of the secondary electron emission coefficient are critical.

VI. FUTURE WORK

The Boltzmann-solver EEDF model developed here can be improved in several ways. The first way to improve the model's accuracy is simply to include more terms in the initial equation (3). Expressions for electron-electron and

electron-ion collisions [19] and for spatial diffusion [17] can be added to eq. (3) without significantly increasing the complexity of the numerical solution. Inelastic collisions other than ionization could also be added to the code, as several cross-sections are readily available for xenon [21]. Of course, the equation could be improved by retaining the time-dependent terms and the spatial gradient terms. The final application of this model may be as the energy equation in a hybrid fluid-PIC simulation of Hall discharges. At the very least, we will continue to use this model in conjunction with a hybrid fluid-PIC simulation (with no feedback) to study the EEDFs for operating conditions and wall materials that have not been explored experimentally.

ACKNOWLEDGMENT

This work was sponsored by the Air Force Office of Scientific Research.

REFERENCES

- [1] G. S. Janes and R. S. Lowder, "Anomalous Electron Diffusion and Ion Acceleration in a Low-Density Plasma," *Phys Fluids* **9**, 1115 (1966).
- [2] J. Fife and M. Martinez-Sanchez, "Comparison of Results from a Two-Dimensional Numerical SPT Model with Experiment," AIAA Paper 96-3197, *32nd Joint Propulsion Conference*, Lake Buena Vista, FL, 1996.
- [3] J. Fife and M. Martinez-Sanchez, "A Numerical Study of Low-Frequency Discharge Oscillations in Hall Thrusters," AIAA Paper 97-3052, *33rd Joint Propulsion Conference*, Seattle, WA, 1997.
- [4] J. P. Boeuf and L. Garrigues, "Low Frequency Oscillations in a Stationary Plasma Thruster," *J. Appl. Phys.* **84**, 3541 (1998).
- [5] E. Fernandez and M. Cappelli, *Bul. Am. Phys. Soc.* **45**, No. 7, 166, *42nd Meeting of the Division of Plasma Physics*, Québec City, Québec, Canada, 2000.
- [6] J. Szabo, M. Martinez-Sanchez, and O. Batishchev, "Numerical Modeling of the Near-Anode Region in a TAL Thruster," AIAA Paper 2000-3653, *36th Joint Propulsion Conference*, Huntsville, AL, 2000.
- [7] V. Yu. Fedotov, A.A. Ivanov, G. Guerrini, A. N. Vesselovzorov, and M. Bacal, "On the Electron Energy Distribution Function in a Hall-type Thruster," *Phys. Plasmas* **6**, 4360 (1999).
- [8] A. I. Bugrova, A. V. Desyatskov, and A. I. Morozov, "Electron Distribution Function in a Hall Accelerator," *Fiz. Plazmy* **18**, 963 (1992) [Translated in *Sov. J. Plasma Phys.* **18**, 501 (1992)].
- [9] A. I. Bugrova, V. S. Versotskii, L. E. Kalikhman, and A. I. Morozov, "Experimental Determination of the Electron Distribution Function in a Plasma Stream," *Teplotiz. Vys. Temp.* **16**, 937 (1978) [Translated in *High Temp.* **16**, 799 (1979)].

- [10] A. I. Bugrova, L. M. Volkova, V. A. Ermolenko, E. A. Kral'kin, A. M. Devyatov, and V. K. Kharchevnikov, "Dynamics of the Electron Energy Distribution Function in a Plasma Accelerator with Extended Acceleration Zone," *Teplofiz. Vys. Temp.* **19**, 1149 (1981) [Translated in *High Temp.* **19**, 822 (1982)].
- [11] N. B. Meezan and M. A. Cappelli, "Optical Study of Anomalous Electron Transport in a Laboratory Hall Thruster," AIAA Paper 99-2284, *35th Joint Propulsion Conference*, Los Angeles, CA, 1999.
- [12] W. A. Hargus, Jr. and M. A. Cappelli, "Interior and Exterior Laser-Induced Fluorescence and Plasma Potential Measurements on a Laboratory Hall Thruster," AIAA Paper 99-2721, *35th Joint Propulsion Conference*, Los Angeles, CA, 1999.
- [13] N. B. Meezan and M. A. Cappelli, "Electron Density Measurements for Determining the Anomalous Electron Mobility in a Coaxial Hall Discharge Plasma," AIAA Paper 2000-3420, *36th Joint Propulsion Conference*, Huntsville, AL, 2000.
- [14] N. P. Carleton and L. R. Megill, "Electron Energy Distribution in Slightly Ionized Air under the Influence of Electric and Magnetic Fields," *Phys. Rev.* **126**, 2089 (1962).
- [15] G. W. Sutton and A. Sherman, *Engineering Magnetohydrodynamics*, New York: McGraw-Hill, pp. 129-138 (1965).
- [16] E. Passoth, J. F. Behnke, C. Csambal, M. Tichy, P. Kudrna, Yu. B. Golubovskii, and I. A. Porokhova, "Radial Behaviour of the Electron Energy Distribution Function in the Cylindrical Magnetron Discharge in Argon," *J. Phys. D.: Appl. Phys.* **32**, 2655 (1999).
- [17] U. Kortshagen, C. Busch, and L. D. Tsengin, "On simplifying approaches to the solution of the Boltzmann equation in spatially inhomogeneous plasmas," *Plasma Sources Sci. Tech.* **5**, 1 (1996).
- [18] S. Yoshida, A. V. Phelps, and L. C. Pitchford, "Effect of Electrons Produced by Ionization on Calculated Electron-Energy Distributions," *Phys. Rev. A* **27**, 2858 (1983).
- [19] D. Uhrlandt, M. Schmidt, and R. Winkler, "A Method to Solve the Nonlinear Kinetic Equation of the "Nonlocal Approach" Including Coulomb Interaction of Electrons," *Comp. Phys. Comm.*
- [20] N. B. Meezan, W. A. Hargus, Jr., and M. A. Cappelli, "Anomalous Electron Mobility in a Coaxial Hall Discharge," *Phys. Rev. E* **63**, 026410-1 (2001).
- [21] CPAT and Kinema Software, www.csn.net/siglo (1998).
- [22] P. H. Dawson, "Secondary Electron Emission Yields of some Ceramics," *J. Appl. Phys.* **37**, 3644 (1966).